The Astrophysical Journal, 678:509–514, 2008 May 1

RADIO SUBMILLIMETER AND γ-RAY OBSERVATIONS OF THE 2003 OCTOBER 28 SOLAR FLARE

G. Trottet,[1] Säm Krucker,[2] T. Lüthi,[3,4] and A. Magun[3,5]

Received 2007 September 27; accepted 2007 December 9

ABSTRACT

Radio observations at 210 GHz taken by the Bernese Multibeam Radiometer for KOSMA (BEMRAK) are combined with hard X-ray and γ-ray observations from the SONG instrument on board *CORONA-F* and the *Reuven Ramaty High Energy Solar Spectroscopic Imager* (*RHESSI*) to investigate high-energy particle acceleration during the energetic solar flare of 2003 October 28. Two distinct components at submillimeter wavelengths are found. The first is a gradual, long-lasting (>30 minutes) component with large apparent source sizes ($\sim 60''$). Its spectrum below $\sim$200 GHz is consistent with synchrotron emission from flare-accelerated electrons producing hard X-ray and γ-ray bremsstrahlung assuming a magnetic field strength of $\geq$200 G in the radio source and a confinement time of the radio-emitting electrons in the source of less than 30 s. The other component is impulsive and starts simultaneously with high-energy (>200 MeV nucleon^{-1}) proton acceleration and the production of pions. The derived radio source size is compact ($\leq 10''$), and the emission is cospatial with the location of precipitating flare-accelerated >30 MeV protons as seen in γ-ray imaging. The close correlation in time and space of radio emission with the production of pions suggests that synchrotron emission of positrons produced in charged-pion decay might be responsible for the observed compact radio source. However, order-of-magnitude approximations rather suggest that the derived numbers of positrons from charged-pion decay are probably too small to account for the observed radio emission. Synchrotron emission from energetic electrons therefore appears as the most likely emission mechanism for the compact radio source seen in the impulsive phase, although it does not account for its close correlation, in time and space, with pion production.

Subject headings: Sun: flares — Sun: particle emission — Sun: X-rays, gamma rays

1. INTRODUCTION

One of the most direct diagnostics of energetic ($\sim$1 MeV) electrons accelerated during solar flares is their synchrotron radiation at centimeter–millimeter wavelengths emitted in magnetic loops associated with the flaring active region (e.g., Pick et al. 1990; Bastian et al. 1998). The electron spectra deduced from the radio emission are generally flat/hard (power-law index $\sim$3), even for weak events (e.g., Kundu et al. 1994), and are consistent with electron spectra inferred from the γ-ray (GR) continuum above $\sim$0.5 MeV (Trottet et al. 1998, 2000). Before the year 2000 no radio observations above 90 GHz were available. At such frequencies the characteristic energy of radiating electrons is of a few MeV in magnetic fields of a few hundred G (e.g., Dulk 1985; Ramaty et al. 1994). Since 2000 new instrumentation observing in the 200–400 GHz range has become available, providing new diagnostics of electrons of a few tens of MeV. These observations are routinely performed by the Solar Submillimeter Telescope (SST) at 212 and 405 GHz (Kaufmann et al. 2001). Furthermore, observations at 230 and 345 GHz have been obtained for two flares by the KOSMA (Köln Observatory for Submillimeter and Millimeter Astronomy) telescope, and one of these flares (2003 October 28) has additionally been observed at 210 GHz by BEMRAK (Bernese Multibeam Radiometer for KOSMA; Lüthi et al. 2004a, 2004b). Both SST at 212 GHz and BEMRAK at 210 GHz provide multibeam measurements that allow us to estimate the location (center of mass) and the averaged size of the millimeter-wave–emitting region. For small X-class flares, these observations show that the synchrotron component extends up to 200 GHz (Trottet et al. 2002) and possibly to higher frequencies (Lüthi et al. 2004b). However, for large X-class flares such as the 2003 November 4 flare (Kaufmann et al. 2004), the 2003 November 2 flare (Silva et al. 2007), and the 2006 December 6 flare (Kaufmann et al. 2007), the radio spectrum above 200 GHz is not the continuation of the synchrotron spectrum measured at lower frequencies, but surprisingly increases with increasing frequency. For these events the radio emission shows fast variations and arises from rather compact sources $\sim 10''$ or less. The emission mechanism of this component with an increasing spectrum is not understood.

In this paper we revisit the radio observations of the 2003 October 28 event discussed by Lüthi et al. (2004a) and perform a multiwavelength analysis including spectral and imaging hard X-ray/γ-ray (HXR/GR) observations obtained by the *Reuven Ramaty High Energy Solar Spectroscopic Imager* (*RHESSI*; Lin et al. 2002) during the decay phase and the measurements of GR emission up to 100 MeV by the SONG instrument on board *CORONA-F* (Kuznetsov et al. 2006).

The 210 GHz emission of the 2003 October 28 flare shows a slowly varying component from the start to the end of the event lasting more than 1 hr and arises from a large source ($\sim 60''$). In addition, a rapidly varying and compact ($\sim 10''$) source is present during a few minutes in the impulsive phase of the flare. Although saturation prevents us from reporting spectral observations at other frequencies during most of the event, the radio spectrum increases with frequency in the decay phase of the extended emission above 210 GHz, while it is consistent with optically thin synchrotron emission at lower frequencies.

2. RADIO AND HXR/GR OBSERVATIONS

The radio observations of the 2003 October 28 flare were obtained in the 19.6–345 GHz domain by different instruments

[1] LESIA, Observatoire de Paris-Meudon, F92190 Meudon, France.
[2] Space Sciences Laboratory, University of California, Berkeley, CA 94720-7450.
[3] Institute of Applied Physics, University of Bern, Sidlerstrasse 5, 3012 Bern, Switzerland.
[4] Leica Geosystem AG, Hexagon Metrology, Moenchmattweg 5, 5035 Unterentfelden, Switzerland.
[5] No longer with IAP.

operated by the Institute of Applied Physics of Bern University (Lüthi et al. 2004a). Total flux densities have been measured at 19.6, 35, and 50 GHz by the Bumishus patrol telescopes, at 89.4 GHz by a nulling interferometer, and at 230 and 345 GHz by KOSMA (Lüthi et al. 2004b). In addition, observations at 210 GHz were made by BEMRAK (Lüthi et al. 2004a), a multibeam instrument that allows us to estimate the location and the size of the 210 GHz emitting region.

2.1. *Time Evolution*

Figure 1 shows the time profiles of the radio flux density at 210 GHz (Lüthi et al. 2004a) and the raw, background-subtracted HXR/GR count rates observed by SONG from 11:00 to 11:12 UT in three energy channels (after 11:12 UT the GR data are contaminated by solar energetic particles). At 210 GHz the time evolution comprises a slowly varying and long-lasting component starting at the beginning of the event ($\sim$11:00:50 UT) to >12:00 UT, and a short-lived and rapidly varying component ($\sim$11:03:50–11:06:05 UT, interval B) exhibiting three peaks with a typical half-power duration of about 20 s. Lüthi et al. (2004a) showed that the long-lasting emission arises from a large source with an effective diameter of $\sim 60''$, while the three impulsive peaks (interval B in Fig. 1) predominantly arise from a compact source with a diameter of $\sim 10''$ and less, which is at a different location (by $\sim 15''$) than that the slowly varying and spatially extended source.

Although there are significant differences in the radio and HXR/GR time profiles, it should be emphasized that (1) the event onset ($\sim$11:02 UT) at 210 GHz is similar to that of the HXR/GR emission below $\sim$20 MeV, and (2) the onset and duration of the radio phase B are similar (within 8 s, the time accumulation used for the >60 MeV GR rate shown in Fig. 1) to those of the >60 MeV GR emission.

During interval A only very faint GR emission (if any) is observed above 60 MeV. This indicates that there is a rollover of the photon spectrum above a few tens of MeV, suggesting that the >10 MeV γ-ray continuum is dominated by electron bremsstrahlung (e.g., Trottet et al. 1998; Vilmer et al. 2003). During intervals B and C, on the other hand, there is significant emission above 60 MeV, indicating a hardening of the >60 MeV photon spectrum. Such a hardening reveals that the high-energy photon spectrum could be predominantly produced by neutral pion decay photons and by bremsstrahlung from high-energy positrons from the decay of charged pions (cf. Vilmer et al. 2003). The production of neutral and charged pions indicates that protons and α particles with energies greater than 200 MeV nucleon^{-1} started to be accelerated at the same time as the onset of the 210 GHz emission with fast time variation observed in interval B. It is noted that the time evolution of the >10 MeV GR emission during the 2003 October 28 flare, which shows a first episode dominated by electron bremsstrahlung followed by an impulsive episode and a long-duration tail dominated by pion decay photons and positron bremsstrahlung, is a sequence that is generally observed during large GR flares (Dunphy et al. 1999; Vilmer et al. 2003).

2.2. *Radio Spectrum*

The only frequency at which the entire time profile of the 2003 October 28 radio event was recorded is 210 GHz. At 89.4 GHz, due to an automatic calibration cycle, the burst observations started only at 11:05:30 UT. The 19.6, 35, 50, 230, and 345 GHz measurements are saturated from $\sim$11:02:20 to 11:16 UT, i.e., during the most intense part of the event. Figure 2 shows the radio spectrum at selected times. The spectrum at

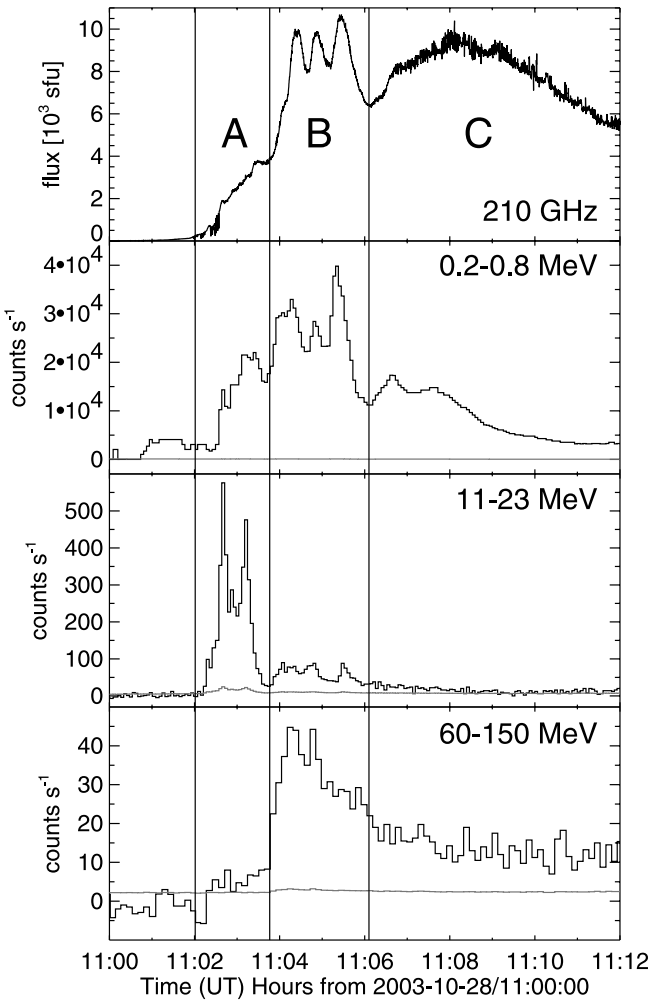

FIG. 1.—Time evolution of the radio flux density (1 sfu $= 10^{-22}$ W m^{-2} Hz^{-1}) at 210 GHz and of the hard X-ray/γ-ray raw count rates (background subtracted) in three energy bands (the thin lines indicate the 1 σ level).

11:02:04 UT (interval A) is reminiscent of optically thin synchrotron emission with a power-law index of $\alpha \sim -1.5$. The spectrum at 11:05:54 UT, which is harder ($\alpha \sim -0.9$), has been obtained in the decay of the third peak in interval B just after the start of the 89.4 GHz observations. The spectra at 11:16:12, 11:25:05, and 11:28:54 UT illustrate the evolution of the radio spectrum during the decay of the event (interval C). As noted by Lüthi et al. (2004a), up to 210 GHz, the radio spectra are consistent with optically thin synchrotron emission with a roughly constant α (-1.1 to -1.3) until $\sim$11:25 UT, and maxima that are always below 50 GHz. In addition to the synchrotron component, the radio spectrum exhibits two remarkable features: (1) after $\sim$11:24 UT the spectrum becomes progressively flatter at frequencies below 210–230 GHz, suggesting an increasing contribution of optically thin free-free emission; and (2) after 11:15:20 UT, when the 345 GHz observations are no longer saturated, the flux density at 345 GHz is about twice the flux density at 210 GHz.

2.3. *Imaging*

BEMRAK observations have been analyzed by Lüthi et al. (2004a) to determine the location and effective angular size of the 210 GHz emitting region during the 2003 October 28 flare. No absolute pointing was available due to a constant but unknown instrumental offset ($\leq 60''$), and no comparison with

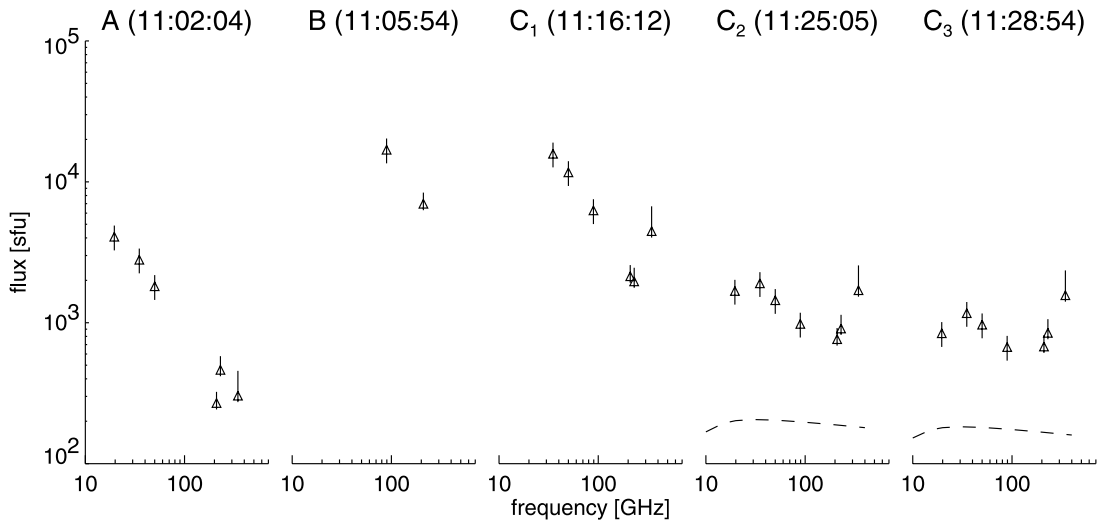

FIG. 2.— Radio spectrum at selected times. Error bars are discussed in Lüthi et al. (2004a). The dashed lines represents the optically thin thermal spectra derived from the *GOES* soft X-ray emission measures and temperatures.

imaging observations in other domains such as EUV and HXR could be done. In order to get absolute pointing for this work we used a full-disk map of the Sun at 210 GHz taken at 11:40 UT (half-power beam width is 88″; see Lüthi et al. 2004b) that still shows flare emission. Together with the location of the solar limb, the absolute position of the 210 GHz flare relative to the Sun's center could be determined. It is rather difficult to determine uncertainties for the absolute pointing, and therefore only a very conservative upper limit is given below. Simulations showed that the accuracy of the relative pointing is better than 10″ (Lüthi et al. 2004a). An additional uncertainty due to the limited tracking accuracy of up to 10″ exists on subsecond timescales. For longer time integrations, however, tracking errors could average to zero, but the details of how this works are not understood. Finally, comparing the postflare emission from the full-disk map with the flare emission seen earlier could also contribute up to 10″. Hence, a very conservative upper limit for the absolute pointing accuracy is ∼30″, but the true accuracy is likely much better.

Using these absolute positions and Figure 9 from Lüthi et al. (2004a), we infer the optimum BEMRAK imaging field of view (size of $\sim 2' \times 2'$ centered at $x = -170''$ and $y = -385''$ from the Sun's center) within which the location and effective angular size of the 210 GHz emitting region can be reliably determined.

Figure 3 presents imaging results in radio, UV, hard X-rays, and γ-rays for the three different time intervals indicated in Figure 1 (*RHESSI* hard X-ray observations are only available for interval C after 11:06 UT). The 2003 October 28 flare is a classic two-ribbon flare with rather long ribbons (>100″) that separate in time as revealed by *TRACE* observations.

At the beginning of the flare (interval A), the 210 GHz emission is located near the southern ribbon and is apparently extended with an average source size of $42'' \pm 10''$ and can be interpreted as a large source that connects the two ribbons, or as a combination of two compact sources, such as two footpoint sources (see Lüthi et al. 2004a for further discussion). Note that, as the northern ribbon is partially outside of the optimal imaging field of view, radio sources from the northern ribbon have less influence on the derived source positions and sizes than the emission from the southern ribbon. The 210 GHz source shows an apparent motion roughly along the ribbons of about 300 km s^{-1}; however, the total motion during interval A is smaller than the average source size. The interpretation of such an apparent motion is difficult, as it could be caused by actual source motion, as well as different temporal intensity variations of subsources.

During interval B when strong pion production is observed, the size of the radio source is much smaller with average values of ∼10″, and the source position is relatively stable and does not change more than ±4″. If the extended source observed in interval A is still present in interval B, although at a low level, the size of the impulsive component alone should be even smaller than values given above. The source location is again near the southern ribbon but shifted by ∼15″ relative to the last position of the radio source in interval A, and it roughly coincides with the flare-averaged 2.2 MeV footpoint position observed on the southern ribbon (Hurford et al. 2006). Although radio emission from the other 2.2 MeV footpoint on the northern ribbon is clearly outside the optimum imaging field of view, it is within one of the multibeams. The derived compact source size therefore suggests that the radio emission from the northern footpoint is much fainter than the emission from the southern footpoint.

During the decay phase (interval C), the radio emission changes location and shape. It arises from an apparently extended source with average size of $57'' \pm 4''$ located between the ribbons, which shows a slow apparent motion of about 25 km s^{-1}. *RHESSI* hard X-ray imaging observations in the 250–450 keV range show two hard X-ray footpoints and a fainter third source in between the footpoints (Hurford et al. 2006). This third source is unlikely a footpoint source but is rather emission from the corona (Krucker et al. 2008), although projection effects do not allow us to unambiguously identify the origin of this source.

3. DISCUSSION

Radio submillimeter imaging of the 2003 October 28 flare reveals the existence of two components with different temporal and spatial behavior: (1) a long-lasting, gradual component with an apparently extended source (∼60″); and (2) an impulsive component originating from a compact source (∼10″). The impulsive component occurs during the phase of strong pion production and originates close to the location of precipitating energetic ions, while the gradual emission comes from an extended coronal source that shows an exponential decay with an *e*-folding time of 200–300 s.

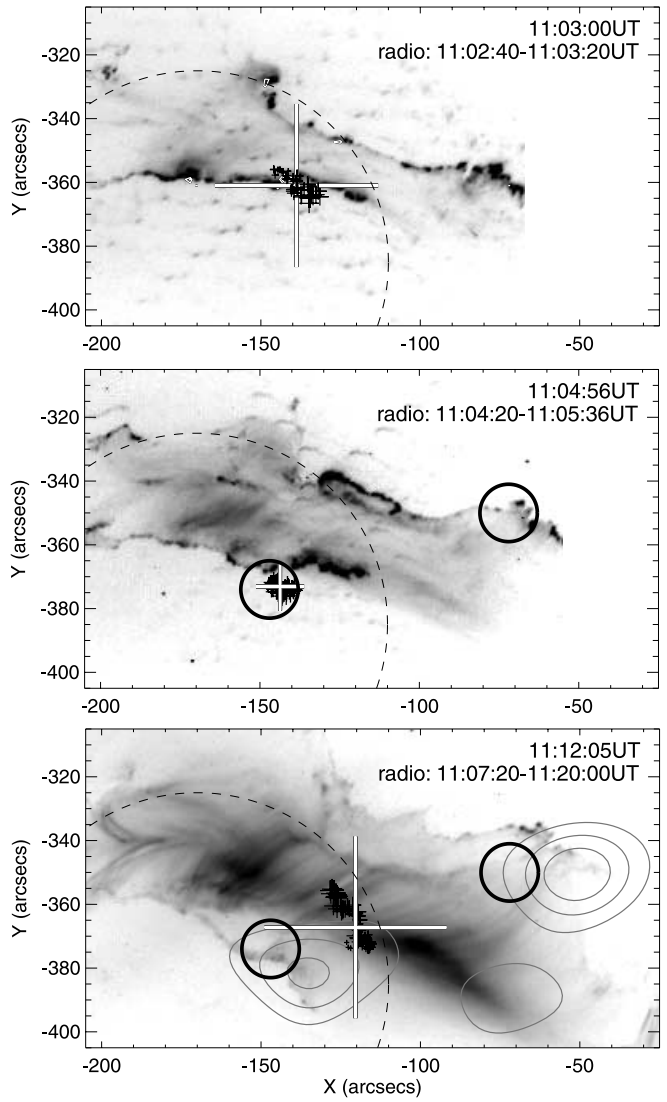

FIG. 3.—Imaging in radio, UV, HXR, and γ-rays during the three time intervals defined in Fig. 1. For each interval, a *TRACE* image is shown (1600 Å for interval A and B; 195 Å for interval C; times are given in the top right corner of each image) with 210 GHz centroid positions overplotted as black crosses (cadence is 10 s; increasing symbol size represents time). The average position and apparent source size of the radio emission during each time interval are represented by a thick white cross. The dashed circle gives a rough size of the field of view of the radio imaging; radio sources outside this circle still influence the derived source position and size but have less weighting than sources within. The thick black circles in the bottom two images give the flare-averaged 2.2 MeV footpoint point location (from Hurford et al. 2006). The circle size represents 1 σ uncertainty in the source location. The bottom image additionally shows *RHESSI* 250–450 keV imaging with 23″ FWHM resolution integrated over the decay phase.

3.1. *Gradual Emission*

Figure 2 shows that above 50 GHz the spectral shape of the gradual component is decreasing with frequency up to ~230 GHz, consistent with optically thin synchrotron emission of relativistic electrons. From the observed spectral index ($\alpha \sim 1.1$–1.3) of the radio observations (§ 2.2), a spectral index of the radio-producing electrons of $\delta \sim 3.2$–3.6 can be derived (e.g., Dulk 1985, their eq. [45]). During the decay phase, HXR/GR emission is observed that also shows exponentially decaying emission on similar timescales (decay time of $\sim 304 \pm 5$ s at 300 keV) as the radio emission. Fits to the GR spectrum reveal that the continuum emission is well represented by a broken power-law spectrum with indices of 2.7 and 2.2, respectively, below and above a break energy of ~0.7 MeV (these values are derived over the total duration of the decay phase 11:06–11:28 UT). Assuming that the HXR/GR emission is produced by bremsstrahlung of energetic electrons in the thick-target approximation (Brown 1971), the flux of electrons above 1 MeV to produce the observed HXR/GR emission around 11:09:30 UT is $F_{\rm GR}(>1\ {\rm MeV}) = 0.15 \times 10^{33}\ {\rm s}^{-1}$. The derived spectral index of above 1 MeV of the GR-producing electrons becomes about 3.2, consistent within uncertainties with the index derived from the radio observations. This suggests that both the radio and >0.7 MeV HXR/GR emission could be produced by the same electron population. In the following, simple order-of-magnitude calculations are presented to investigate what magnetic field strength and confinement/trapping times of radio-emitting electrons are needed to match both the observed GR and radio fluxes. For simplicity, the presented calculations are only done at a single time (11:09:30 UT). For different values of the magnetic field strength B in the radio source, the number of electrons above 1 MeV, $N_R(>1\ {\rm MeV})$, are derived (Table 1) using the Ramaty gyrosynchrotron code (Ramaty et al. 1979; Kozlovsky et al. 2002). For a given value of B, the confinement time Δt of the radio producing (i.e., ~1 MeV) electrons becomes $\Delta t \approx N_R(>1\ {\rm MeV})/F_{\rm GR}(>1\ {\rm MeV})$ (e.g., Ramaty et al. 1994). The collisional loss time $\tau_{\rm coll}$ displayed in Table 1 has been computed for the characteristic energy of 210 GHz emitting electrons, $E_{\rm char}$, and for an ambient density of 10^{11} cm^{-3}, a value deduced from thermal X-ray observations by *RHESSI*. For an observing frequency $\nu_{\rm obs} = 210$ GHz, $E_{\rm char}$ is given approximately by $E_{\rm char}({\rm MeV}) \sim 0.511(\nu_{\rm obs}/\nu_B - 1)^{0.5} \sim 140 B^{-0.5}$, where $\nu_B({\rm GHz}) = 2.8 \times 10^{-3}\ B$ (G) is the electron gyrofrequency (cf. Dulk 1985). Here $\tau_{\rm syn}$ is the synchrotron loss time for electrons of energy $E_{\rm char}$. Although *RHESSI* observes HXR/GR emission from the corona (Fig. 3, *bottom*), no emission is seen at the location of the gradual 210 GHz source. This indicates that HXR/GR emission from the gradual radio source is <20% of the total HXR/GR emission. In the thin target approximation, this limit gives an upper limit for the instantaneous number of >1 MeV electrons in the radio source of $\sim 1 \times 10^{33} (10^{11}\ {\rm cm}^{-3}/n_{\rm amb})$, where $n_{\rm amb}$ is the ambient density. Comparing this upper limit with the derived number of electrons in the radio source in Table 1, the magnetic field strength has to be above 400 G for densities of 10^{11} cm^{-3} and above 150 G for densities of 10^{10} cm^{-3}. For very high magnetic fields (>1000 G), electrons do not need to be confined in the radio source, as the transit time across the radio source ~0.3 s is

TABLE 1
PARAMETERS OF 210 GHz RADIO-EMITTING REGION DURING THE GRADUAL EMISSION

B (G)	N_R (>1 MeV) (10^{33})	$E_{\rm char}$ (MeV)	Δt (s)	$\tau_{\rm coll}$ (s)	$\tau_{\rm syn}$ (s)
50	60	20	400	530	4900
100	15	15	100	380	1700
200	4	10	27	270	570
300	1.5	9	10	230	300
400	0.75	8	5	200	190
500	0.5	7	3	180	130
700	0.25	6	1.5	150	80
1000	0.1	5	0.7	130	40

NOTE.—See text.

of the same order of magnitude as the confinement time. Therefore, the coronal magnetic field strength in the gradual 210 GHz source should be between $\sim$200 and $\sim$1000 G.

Toward the end of the decay phase (after 11:24 UT) the radio spectrum is progressively flattening below $\sim$200 GHz, suggesting that optically thin thermal emission contributes to the radio emission. Thermal soft X-ray observations from *GOES* were used to estimate the optically thin thermal radio emission for these later times. The calculated thermal spectra shown in Figure 2 as dashed curves suggest that indeed optically thin radio emission contributes significantly. The comparison of spectra at 11:25 and 11:28 UT shows that the synchrotron component is faster decaying than the thermal emission, further corroborating that the spectral flattening below 200 GHz is at least partly due to the thermal emission that becomes more and more important at progressively later times.

At 345 GHz, the radio spectrum is increasing again, as observed during the impulsive phase of most of the few events so far observed at these high frequencies (Kaufmann et al. 2004, 2007; Silva et al. 2007). Optically thick thermal emission would have the right spectral shape to explain such increasing spectra (Ohki & Hudson 1975). For a spherical source of 60″ diameter and a flux density of 5000 sfu (1 sfu = 10^{-22} W m^{-2} Hz^{-1}) at 345 GHz (the maximum flux density observed after saturation) optically thick free-free emission requires a temperature of $\sim$0.2 MK and a medium density of $\gg 2 \times 10^{11}$ cm^{-3}. This implies a thermal energy content of $\gg 10^{30}$ erg for the 0.2 MK radio-emitting plasma. This is only a small fraction of the total integrated irradiance for the 2003 October 28 flare, $(6 \pm 3) \times 10^{32}$ erg (Kopp et al. 2005). Optically thick thermal emission thus provides a plausible explanation for increasing radio spectra above 210 GHz during the gradual phase.

Finally, it should be emphasized that HXR/GR and radio emissions during the gradual phase of the 2003 October 28 flare imply continuous acceleration of high-energy particles (electrons and ions) at the Sun. This is consistent with the finding by Li et al. (2007) that progressive magnetic reconnection associated with the slow separation of the flare ribbons observed during this event plays a major role in the acceleration of these particles.

3.2. *Impulsive Emission*

As the 345 GHz measurements are saturated, the spectral shape above 210 GHz is unknown for the impulsive emission. Hence, it is not known whether the radio spectrum above 210 GHz continues to decrease, as was observed for a few flares (Trottet et al. 2002; Lüthi et al. 2004b; Guiménez de Castro et al. 2005), or increases with frequency, as was reported for very large flares like the present one (Kaufmann et al. 2004, 2007; Silva et al. 2007). In the latter case, the emission at 210 GHz could contain contributions from both the decreasing component and the increasing component. In the following we discuss the different possibilities assuming that the 210 GHz emission arises entirely from the compact source. This leads to an upper limit of $\sim 10^4$ sfu for the flux density of the compact source at 210 GHz during interval B.

3.2.1. *Decreasing Spectrum above* 210 GHz

A decreasing radio spectrum with increasing frequency is consistent with optically thin gyrosynchrotron emission. Since the flux density and spectral shape (between 89.4 and 210 GHz) of the impulsive phase are observed to be of the same order of magnitude and similar as for the gradual phase, the number of needed energetic electrons are also of the same order of magnitude as for the gradual phase (see Table 1). Since no *RHESSI* observations are available for the impulsive phase, no detailed comparison can be done. However, SONG observations show that the HXR/GR emission in the impulsive phase is larger than during the gradual phase, and the number of hard X-ray–producing electrons is therefore likely to be larger as well. This indicates that optically thin synchrotron emission leads to acceptable numbers of radiating electrons and magnetic field strength to produce the compact source at 210 GHz during the impulsive phase. For $\alpha \sim -0.9$ a maximum flux density of $\sim$6400 sfu is expected at 345 GHz.

3.2.2. *Increasing Spectrum above* 210 GHz

In the following we qualitatively comment on three possibilities that may potentially explain the spectral inversion above $\sim$200 GHz: Razin-suppressed synchrotron emission from (1) high-energy electrons or (2) positrons, and (3) optically thick free-free emission. For the calculations below we assume that, like in other events, the slope of the radio spectrum above 200 GHz is about 1. For a maximum flux density of 10^4 sfu at 210 GHz this leads to an expected maximum flux density of $\sim 1.6 \times 10^4$ sfu for the compact source at 345 GHz.

1. For $\sim 1.6 \times 10^4$ sfu at 345 GHz and an increasing spectrum above 210 GHz the available data do not provide enough constraints to determine a unique set of parameters [B, $n_{\rm amb}$, $N_R(>1\ {\rm MeV})$]. As an illustration, this can be achieved for $B =$ 700 G, $n_{\rm amb} = 8 \times 10^{12}$ cm^{-3}, and $N_R(>1\ {\rm MeV}) = 5 \times 10^{33}$. Such parameters imply an efficient Razin suppression below 220 GHz. Hence, optically thin synchrotron emission from 1–10 MeV electrons could explain increasing spectra above $\sim$200 GHz. Such an emission from a compact, high-density and high-magnetic field region does not contribute substantially to the radio emission below $\sim$220 GHz.

2. The possibility to produce microwave emission by positrons was first pointed out by Lingenfelter & Ramaty (1967). This is an attractive possibility for the present event because the compact radio source starts simultaneously with pion production (cf. § 2.1) and roughly coincides with one of the 2.2 MeV footpoints, i.e., with one interaction region of accelerated protons/ions (cf. § 2.3). A detailed modeling of the radio source in terms of positrons is beyond the scope of this paper. As a first approach, the positron spectrum can be taken constant between 15 and 100 MeV and 0 elsewhere, as shown in Figure 2 of Lingenfelter & Ramaty (1967). For comparison, we first adopted the same values as above ($B =$ 700 G and $n_{\rm amb} = 8 \times 10^{12}$ cm^{-3}). For these values, the synchrotron emission from positrons is Razin suppressed at 210 GHz, so that the 210 GHz emission originates almost entirely from optically thin synchrotron emission from electrons as discussed in § 3.2.1. The required flux density of 1.6×10^4 sfu at 345 GHz is achieved for a total number of positrons of $\sim 10^{33}$. On the other hand, for $n_{\rm amb} = 10^{12}$ cm^{-3}, Razin suppression only starts to be important below 40 GHz, and both the 210 and 345 GHz emissions are entirely due to synchrotron emission from positrons. For this latter case, a total number of 6×10^{31} positrons is needed to match the required flux densities. The number of positrons produced by >200 MeV protons is 10^{-2} to 10^{-1} per proton (see Fig. 3 in Lingenfelter & Ramaty 1967). Therefore, at least 6×10^{32} protons with energies larger than 200 MeV are needed to account for the radio emission. This is 1–2 orders of magnitude larger than the range of values derived to account for one of the largest fluxes of pion-decay photons detected during the 1990 May 24 flare (Vilmer et al. 2003). The above simple analysis shows that synchrotron radiation by positrons from charged-pion decay is likely to be too small to

account for the observed 210 GHz emission (see also Silva et al. 2007). However, to definitively exclude this possibility, further analysis of similar flares with complete spectral coverage, together with detailed modeling including particle transport and directivity effects, and more precise calculation of positron yield are needed.

3. As mentioned in § 3.1, optically thick thermal free-free emission is a possibility to produce a radio spectrum that increases with frequency (Ohki & Hudson 1975). Assuming that the diameter of the 345 GHz source is similar to that of the 210 GHz source ($<10''$), this leads to a temperature of $\sim 3.5 \times 10^7$ K, and an emission measure of $\gg 8 \times 10^{52}$ cm^{-3}, thus an ambient electron density of $\gg 2 \times 10^{13}$ cm^{-3} in the radio-emitting region. For an isothermal source the soft X-ray observations by *GOES* provide a comparable maximum temperature (2.5×10^7 K), but the emission measure of $\sim 10^{51}$ cm^{-3} is almost 2 orders of magnitude lower. Furthermore, such a high density is unusual at such high temperatures. With these parameters a magnetic field $B \gg$ 2000 G is needed to have a low β (gas pressure to magnetic pressure ratio). Such an unlikely combination of parameters indicates that optically thick thermal free-free emission has to be excluded.

3.2.3. *Summary*

While the 210 GHz radio emission from the compact source during the impulsive phase is inconsistent with optically thick free-free emission, optically thin synchrotron emission from 1–10 MeV electrons may account for the 210 GHz observations. If, as is observed in other large flares, the radio spectrum increases with frequency above 210 GHz, this additional emission may arise from synchrotron emission by an additional electron population in a compact source with high density and high magnetic field. However, such a scenario does not explain why the 210 GHz source switches on when strong pion production starts and is cospatial with a 2.2 MeV line source, i.e., with a region of ion interaction that may be displaced from the main electron interaction region. Although, synchrotron emission from pion decay positrons would be consistent with these latter facts, simple order-of-magnitude estimations show that such an emission is likely to be too faint (by 1–2 orders of magnitudes) to account for the observed fluxes. A further argument against synchrotron emission from pion decay positrons is that the third 210 GHz peak around 11:05:20 UT is not seen in the 60–150 MeV time profiles. However, more detailed calculations taking into account the directivity of both the GR submillimeter emissions are needed, and more events should be analyzed before synchrotron emission from pion decay positrons can be definitively ruled out. A further possibility that should be explored quantitatively is emission from proton beams as proposed by Smith & Benz (1991) and Sakai & Nagasugi (2007). Finally, it should be remarked that the onset of the compact source at 210 GHz, which is at a different location than the spatially extended and long-lasting source, is a signature that a new magnetic structure is involved in particle acceleration and transport leading to an increases production of high-energy electrons and to the onset of high-energy ion (>200 MeV nucleon^{-1}) acceleration. This is in line with the results of multiwavelength studies, which provided evidence that interaction between two or more magnetic loops is a basic driver to trigger efficient acceleration of high-energy particles (e.g., Raoult et al. 1985; Chupp et al. 1993; Trottet et al. 1994, 2006; Shibasaki 2001).

The work of G. T. has been supported by Centre National de la Recherche Scientifique and Centre National d'Études Spatiales. S. K. has been supported through NASA contract NAS 5-98033 for *RHESSI*. We are grateful to A. L. MacKinnon and H. S. Hudson for their comments and suggestions. We also thank K. Kudela, V. Kurt, and I. Myagkova for providing the SONG observations. SONG measurements and data analysis in Slovakia are supported by the Slovak Research and Development Agency under the contract No. APVV-51-053805.

REFERENCES

Bastian, T. S., Benz, A. O., & Gary, D. E. 1998, ARA&A, 36, 131
Brown, R. L. 1971, Sol. Phys., 18, 489
Chupp, E. L., Trottet, G., Marschhauser, H., Pick, M., Soru-Escaut, L., Rieger, E., & Dunphy, P. P. 1993, A&A, 275, 602
Dulk, G. A. 1985, ARA&A, 23, 169
Dunphy, P. P., Chupp, E. L., Bertsch, D. L., Schneid, E. J., Gottesman, S. R., & Kanbach, G. 1999, Sol. Phys., 187, 45
Giménez de Castro, C. G., et al. 2005, in AIP Conf. Proc. 784, Magnetic Fields in the Universe (New York: AIP), 566
Hurford, G. J., Krucker, S., Lin, R. P., Schwartz, R. A., Share, G. H., & Smith, D. M. 2006, ApJ, 644, L93
Kaufmann, P., et al. 2001, in IAU Symp. 203, Recent Insights into the Physics of the Sun and Heliosphere, ed. P. Brekke, B. Fleck, & J. B. Gurman (San Francisco: ASP), 283
———. 2004, ApJ, 603, L121
———. 2007, BAAS, 210, 93.30
Kopp, G., Lawrence, G., & Rottman, G. 2005, Sol. Phys., 230, 129
Kozlovsky, B., Murphy, R. J., & Ramaty, R. 2002, ApJS, 141, 523
Krucker, S., Hurford, G. D., MacKinnon, A., L. Shih, A. Y., & Lin, R. P. 2008, ApJ, 678, L63
Kundu, M. R., White, S. M., Gopalswamy, N., & Lim, J. 1994, ApJS, 90, 599
Kuznetsov, S. N., Kurt, V. G., Myagkova, I. N., Yushkov, B. Y., & Kudela, K. 2006, Sol. Syst. Res., 40, 104
Li, C., Tang, Y. H., Dai, Y., Fang, C., & Vial, J.-C. 2007, A&A, 472, 283
Lin, R. P., et al. 2002, Sol. Phys., 210, 3
Lingenfelter, R. E., & Ramaty, R. 1967, Planet. Space Sci., 15, 1303
Lüthi, T., Lüdi, A., & Magun, A. 2004a, A&A, 420, 361
Lüthi, T., Magun, A., & Miller, M. 2004b, A&A, 415, 1123
Ohki, K., & Hudson, H. S. 1975, Sol. Phys., 43, 405
Pick, M., Klein, K.-L., & Trottet, G. 1990, ApJS, 73, 165
Ramaty, R., Kozlovsky, B., & Lingenfelter, R. E. 1979, ApJS, 40, 487
Ramaty, R., Schwartz, R. A., Enome, S., & Nakajima, H. 1994, ApJ, 436, 941
Raoult, A., Pick, M., Dennis, B. R., & Kane, S. R. 1985, ApJ, 299, 1027
Sakai, J. I., & Nagasugi, Y. 2007, A&A, 470, 1117
Shibasaki, K. 2001, ApJ, 557, 326
Silva, A. V. R., et al. 2007, Sol. Phys., 245, 311
Smith, D. F., & Benz, A. O. 1991, Sol. Phys., 131, 351
Trottet, G., Chupp, E. L., Marschhaeuser, H., Pick, M., Soru-Escaut, I., Rieger, E., & Dunphy, P. P. 1994, A&A, 288, 647
Trottet, G., Correia, E., Karlický, M., Aulanier, G., Yan, Y., & Kaufmann, P. 2006, Sol. Phys., 236, 75
Trottet, G., Raulin, J.-P., Kaufmann, P., Siarkowski, M., Klein, K.-L., & Gary, D. E. 2002, A&A, 381, 694
Trottet, G., Rolli, E., Magun, A., Barat, C., Kuznetsov, A., Sunyaev, R., & Terekhov, O. 2000, A&A, 356, 1067
Trottet, G., Vilmer, N., Barat, C., Benz, A., Magun, A., Kuznetsov, A., Sunyaev, R., & Terekhov, O. 1998, A&A, 334, 1099
Vilmer, N., MacKinnon, A. L., Trottet, G., & Barat, C. 2003, A&A, 412, 865